06

Effect of strain on thermoemf in the silicate glass doped with ruthenium dioxide

© M. Tursunov,[1] A. Dekhkonov,[1] G. Abdurakhmanov,*[1] V. Ksenevich,[2] D. Tashmukhamedova,[3] G. Vokhidova,[4] Dibya Prakash Rai[5]

[1]National University of Uzbekistan named after Mirzo Ulugbek,
100174 Tashkent, Uzbekistan
[2]Belarusian State University,
220030 Minsk, Republic of Belarus
[3]Tashkent State Technical University,
100095 Tashkent, Uzbekistan
[4]Nonstate Training Center „Alphacom“,
100084 Tashkent, Uzbekistan
[5]Pachhunga University College, Pachhunga,
796001 Aizawl Mizoram, India
e-mail: gulmirzo@mail.ru

Received November 6, 2024
Revised February 19, 2025
Accepted March 19, 2025

The effect of uniaxial strain on the thermoEMF of the ruthenium dioxide-doped silicate glass (thick film resistor) was studied. The variation of the thermoEMF has been analysed based on the dopant compositions and applied strain. We comprehensively studied a doped sample's complex matrix concerning the atoms' radial distribution. We report the enhanced value of the thermoEMF in the deformed sample by 20−120 times larger than the unstrained one. We have measured the ratio of the strained-induced thermoEMF and the resistance in a complex matrix with the lowest atomic arrangement. However, the highest coefficient of thermoEMF (Seebeck coefficient) has been found in the simplest glass composition. ThermoEMF measured in the doped silicate glass is sensitive to the measuring tool.

Keywords: Seebeck coefficient, strain gauge coefficient, strain sensor, three-point bending installation, piezoresistive effect

DOI: 10.61011/TP.2025.07.61458.405-24

Introduction

Strain sensors play an important role in various fields of investigations and industry, including materials science, aerospace industry, robotics, automotive industry, agriculture and medicine [1–3]. The widely-used strain sensors are based on variation of electrical resistance of a material due to strain (piezoresistive sensors). These sensors are classified as wire, metal-foil, semiconductor, thin-film and thick-film ones. The wire and the metal-foil sensors [4–6] are ones of the oldest and most reliable strain sensors and are available in various forms. These sensors have high temperature stability (the temperature coefficient of resistance is about $10 \cdot 10^{-6}\,\mathrm{K}^{-1}$), while their low sensitivity to strain (the strain gauge coefficient GF is within 2−4) requires to use complicated amplification circuits [1,2]. On the contrary, the semiconductor sensors have a high strain gauge coefficient (about 150) [1], but their temperature sensitivity is also high ($\mathrm{TCR} \approx 90000 \cdot 10^{-6}\,\mathrm{K}^{-1}$). In the thin-film strain sensors, sensitive materials can be metals, semiconductors and ceramics [5,7–9]. Properties of the thin-film sensors manufactured of metals and alloys are similar to characteristics of the metal-foil sensors. The thin-film strain sensors are preferable tools for measuring strain in small-size devices due to their high reliability, long-term stability and excellent accuracy [9–11]. The thick-film resistive sensors are in a mid position with $GF = 10 - 20$ and $\mathrm{TCR} = (50 - 100) \cdot 10^{-6}\,\mathrm{K}^{-1}$ [2,12–15]. Physically, the term „piezoresistive“ means change of sensor resistance due to strain.

$$R = \rho l / s, \tag{1}$$

where ρ, l and s — resistivity, a sensor length and a cross-sectional area of the material, respectively.

The relative resistance change (ΔR) can be expressed via relative changes of ρ, l and s:

$$\Delta R/R = \Delta\rho/\rho + \Delta l/l - \Delta s/s, \tag{2}$$

where $\Delta R = R - R_0$, $\Delta l = l - l_0$, $\Delta s = s - s_0$, R_0, l_0, and s_0 — the initial values (without strain), R, l and s are parameters with taking into account sensor strain. The main cause of variation of resistance of the wire and the metal-foil sensors is variation of the geometrical parameters l and s, whereas ρ remains virtually constant, so

$$GF_R = (\Delta R/R_0)/\varepsilon \approx 2, \tag{3}$$

Table 1. Composition of the studied DCG samples (mass%)

Sample	Glass components								T_f/τ_f, K/h	The ligature (RuO_2)
	SiO_2	PbO	Al_2O_3	BaO	CuO	MnO_2	B_2O_3	MgO		
1	33.0	67.0							1773/1	30.0
2	27.0	67.0		4.0				2.0	1673/1	20.0
3	11.0	61.9	0.7		1.4	10.0	15.0		1623/1	30.0

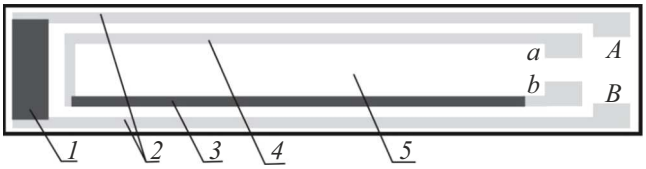

Figure 1. Thick-film thermoelectric strain gauge: *1* — the thick-film heater; *2* — the metal (Ag+Pd) contacts; *3* — the doped-glass layer (the thermocouple branch); *4* — the metal (Ag+Pd) contact (the second thermocouple branch); *5* — the ceramic substrate (96 % Al_2O_3). The contacts *A* and *B* are used to connect a heating current source, the contacts *a* and *b* are used to connect to a nanovoltmeter or an ohmmeter.

where $\varepsilon = \Delta l/l_0$ longitudinal strain of the sensor, while the material volume $V_0 = l_0 \cdot s_0$ is assumed to be constant (Δl and Δs are small values).

There is another strain-sensitive physical property — a thermoelectric effect (Seebeck effect), which is often used for measuring the temperature and detecting structural transitions that occur at high pressures as well as for detecting hidden structural transitions. The dependence of the thermoEMF on the structural transitions was also detected in thick-film resistors [15,16] that are made of silicate glass doped with oxides of the transition metals (DSG). At this, variation of the thermoEMF value was approximately in ten times higher than variation of the resistance. The structural transitions of the papers [15,16] were caused by temperature variation, which makes it impossible to evaluate these materials as sensitive elements of the strain sensors. However, publications do not contain data about the dependence of the thermoEMF on strain in the thick-film DSG-based resistors. The present study has tried to fill this gap and evaluate the thermoEMF in DSG as a tensometric property and discusses possible physical mechanisms of strain sensitivity of the thermoEMF of these materials.

1. Experiment

Fig. 1 shows an arrangement of the DSG sample for simultaneous measurement of strain sensitivity of the thermoEMF and the resistance. The samples are manufactured by a standard technology of the thick-film resistors: submicron powders of glass and dopant oxide (Table 1) were mixed with addition of an organic carrier, screen-printed to a ceramic substrate and baked for τ_f at the maximum temperature T_f. The ceramic substrate (96 % Al_2O_3) had the sizes $420 \times 4 \times 0.3$ mm. The metal electrodes were made of a conducting silver paste PP-1 produced by LLC Elma-pasty (Zelenograd, Russia). The heater *1* with resistance of about $340 - 830\,\Omega$ was made of glass of the composition 3 (Table 1) with the mass fraction of RuO_2 of 40 %.

The distribution of the temperature along the thermoelectric element *2*, that is created by the heater *1*, was controlled by the thermal imager Fluke Ti 450 Pro (the accuracy of about 2 K wit the sensitivity of at least 0.05 K). In all the experiments, the temperature difference between a hot and a cold side of the element 2 was 33 K. The contacts *A*, *B*, *a* and *b* were at the room temperature and connected the sample with an electric current source for heating and with a thermoEMF and resistance meter (the nanovoltmeter 2182A Keithley and the multimeter DM3058 RIGOL, respectively).

The uniaxial strain (compression or tension) of the samples was created using a three-point diagram (Fig. 2) [13] and the homemade experimental installation (Fig. 3). Here

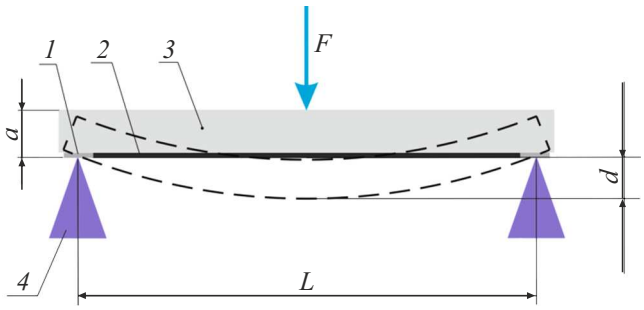

Figure 2. Diagram of creating uniaxial strain when measuring variations of the thermoEMF and the resistance. The ceramic substrate *3* is supported at both sides (upper and lower) in clamps *4*. The load *F* is applied in the middle of the substrate by means of a movable clamp, thereby creating tension or compression depending on a direction of the force *F*. The bending test diagram: *1* — the fixed rest point, *2* — the heater and the studied thick-film thermocouple, *3* — the substrate, *4* — the fixed supports

Figure 3. Homemade installation for measuring influence of strain on the thermoEMF of the thick-film thermoelectric sensor: *1* — the sample holder, *2* — the movable clamp, *3* — the handle for moving the clamp *2*, *4* — the handle for moving the micrometer *5*.

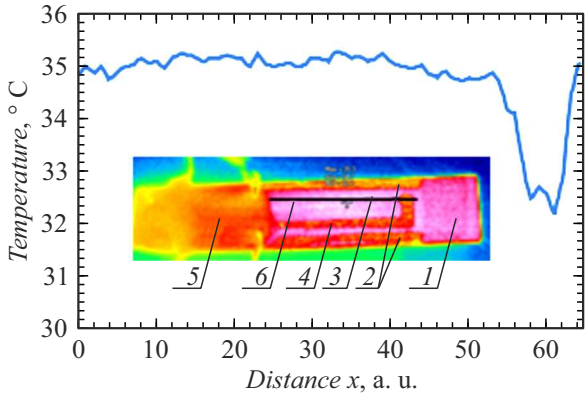

Figure 4. Distribution of the temperature along the element of the sensor 3 (the line 6 of the insert). The element *3* of the sensor was heated by transmission of the electric current. The insert: a thermal image of the thermoelectric sensor shown in Fig. 1. The designation *1*–*5* are the same as in Fig. 1.

d is the sample deflection measured by the dial gauge 1MIG (Russia) with the resolution of $1\,\mu$m. The samples composition and the distribution of the elements along the surface were analyzed by means of the scanning-electron microscope JEOL JSM-IT200 with the energy-dispersive spectrometer (Uzbek-Japan Center of Youth Innovations, Tashkent State Technical University).

The strain value is determined by the equation [13,14]:

$$\varepsilon = \Delta l/l = 6ad/L^2, \qquad (4)$$

where a — the substrate thickness, [m], d — the deflection, [m], and L — the distance between the support edges *4*, [m], in Fig. 2. The thickness of the thick-film layer is about $25\,\mu$m, which is neglected in comparison with the thickness of the substrate 4 ($a = 300\,\mu$m). It should be noted that the Young's modulus is about ~ 300 GPa [17], which is substantially higher than that of the glass (~ 70 GPa) [18], so the glass layer strain will correspond to strain of the substrate surface, on which this layer is arranged.

It should be noted that uniformity of the thermoelectric material is an important factor affecting generation of the thermoEMF [19,20]. In order to find a degree of nonuniformity of the DSG layer *3* (Fig. 1) and generation of the spurious thermoEMF related thereto, we have studied the distribution of the temperature along this layer when heating it by transmission of the electric current (Fig. 4), while the heater *1* was turned off. As it can be seen from Fig. 4, the temperature gradients in the layer *3* of the doped glass do not exceed 0.5 K and can not noticeably contribute to the measured thermoEMF (we remind that the sensitivity of the thermal imager Fluke Ti 450 Pro is at least 0.05 K).

2. Results and discussion

The dependence of the resistance R and the thermoEMG U_T of the DSG samples given in Table 1 on the strain is shown in Fig. 5. These graphs demonstrate symmetry and high linearity of $U_T(\varepsilon)$ and $R(\varepsilon)$ for all the studied DSG compositions.

The values of the resistance R_0 and the thermoEMF U_{T0} of the non-strained samples and the strain gauge coefficients GF_R and GF_{UT} that are calculated from the measured values of $R(\varepsilon)$ and $U_T(\varepsilon)$ were given in Table 2. We note that:

1) in all the cases GF_{UT} exceeds GF_R in 20–120 times;

2) the lower the content of RuO_2 in the composition the higher GF_{UT}, whereas GF_R is lower; the correlation is opposite;

3) the value of U_{T0} does not correlate to GF_{UT}, whereas there is direct correlation between R_0 and GF_R;

4) the glass composition (Table 1) greatly affects the strain gauge coefficient GF_{UT}, but this correlation requires more detailed research.

Many researchers have studied the piezoresistive effect in the thick-film resistors [11–14,21–34]. The most of these studies were performed on commercially available resistors and correlation between the strain sensitivity and the composition of the resistors was not described. At the same time, there were attempts to explain these properties [27–35] via resistor microstructures. However, these studies were unsuccessful as it was assumed that a mechanism of conductivity in the thick-film resistor was attributed to a charge flowing along a chain of mutually contacting ligature particles with high electrical conductivity (mainly RuO_2 and ruthenates of bismuth, lead) and

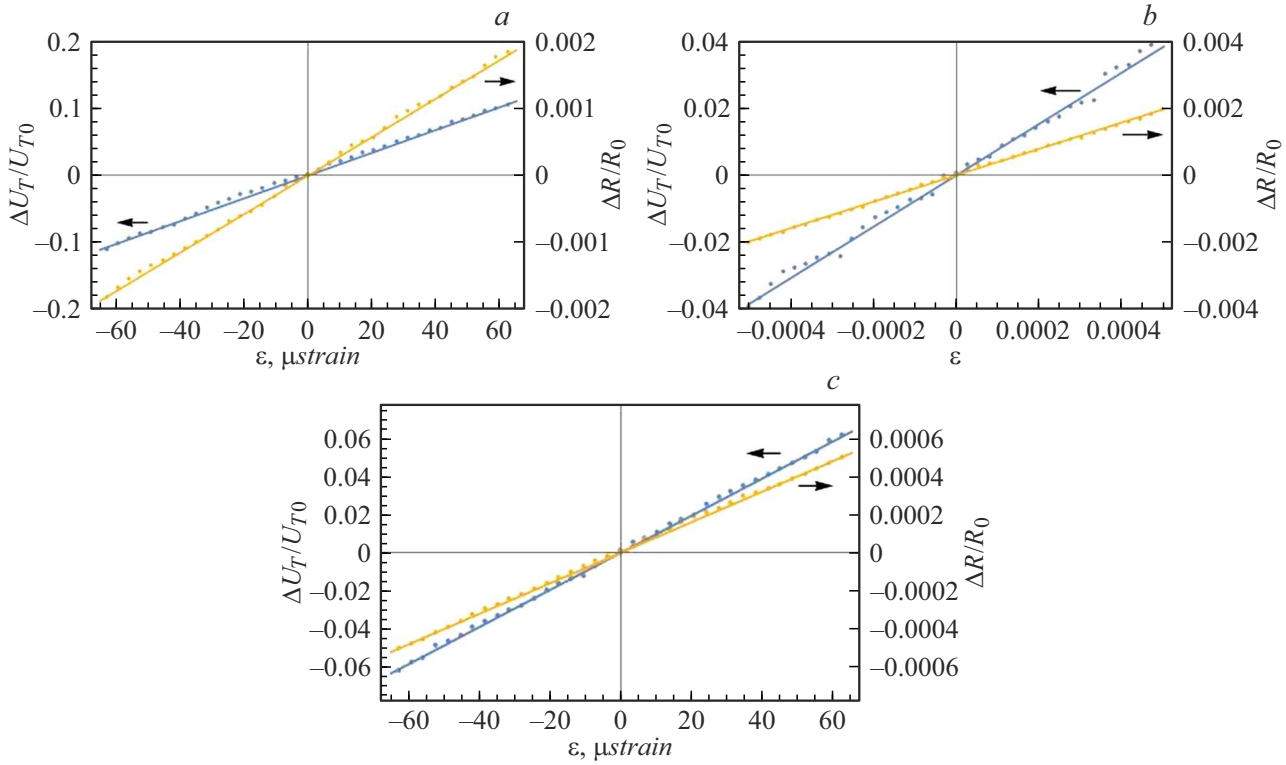

Figure 5. Dependence of the resistance and the thermoEMF on relative strain for the compositions of the doped glass: *a* — 1, *b* — 2, *c* — 3.

Table 2. Initial (in a non-strained state) values of the resistance R_0 and the thermoEMF U_{T0}, the strain gauge coefficients of the resistance GF_R and the thermoEMF GF_{UT} of the studied samples

Sample	R_0, Ω	U_{T0}, μV	S, μV/K	GF_R	GF_{UT}	GF_{UT}/GF_R
1	1199	306	9.3	29	1673	58
2	3646	217.1	6.6	31	661	21
3	166.6	1.184	0.036	7.9	973	123

tunneling or jumps of the charge carriers between these particles. This approach considers the glass in DSG as an inert matrix, in which the ligature particles are distributed quite evenly. In accordance with a flowing theory, when the volume content of the ligature is about 16 % (the critical volume C_c) or more in the three-dimensional system, the ligature particles can contact each other to form an endless conducting cluster [36]. It is assumed that the piezoresistive effect is caused by a change of the area of contacting surfaces of the ligature particles. This assumption of the structure and the properties of the DSG is based on electron-microscopic images and an X-ray diffraction pattern, which exhibit crystal particles of the ligature. There is an opposite point of view about the nature of high sensitivity of silicate glass doped by RuO_2 to strain: Totokawa et al. in the studies [37–39] have shown that the thin film of glass based on bismuth-borosilicate rhutenium-doped glass

1) contains both three-valence and tetra-valence states of rhutenium;

2) exhibits conductivity that can be described as jumps with a variable hole length;

3) demonstrates high sensitivity to strain due to spatial expansion of the wave function of the carriers (holes) in the localized states;

4) the Ru atoms diffuse into the glass during baking;

5) the diffusion constant of Ru diffusing into the bismuth-borosilicate glass is $1.4 \cdot 10^{-13}\,\mathrm{m^2/s^{-1}}$, while the diffusion length is 100 nm;

6) the piezoresistive characteristics depend on the distance to the interface of the glass layers and RuO_2.

This approach has several contradictions with the experiments:

1) the percolation threshold as well as the resistivity depend on the glass composition, the baking temperature

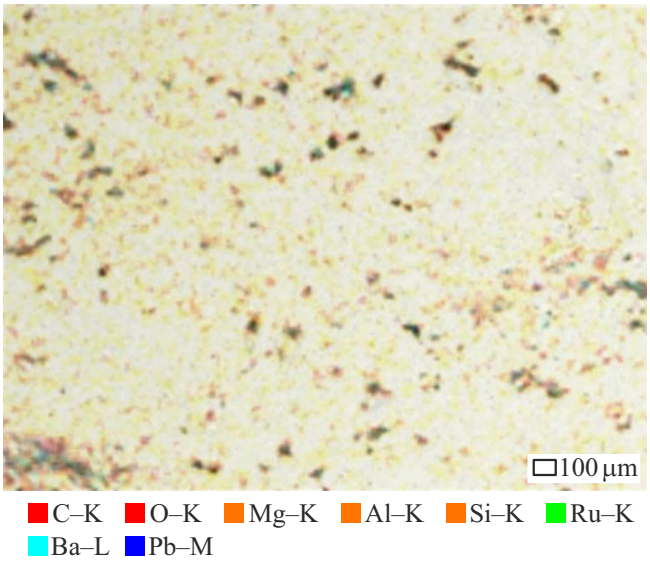

Figure 6. Distribution of the elements on the surface of the doped glass of the composition 2 as obtained by the energy-dispersive spectrometer. It is clear that the RuO_2 particles are arranged at a large distance from each other and do not contact each other.

T_f and the baking time τ_f [29], which is not typical for the flowing theory;

2) the percolation threshold can shift towards a lesser content of a dopant (1–5 vol%) contrary to theoretical predictions ($C_c \approx 16$ vol%), or it can even disappear [40];

3) the estimated real interparticle distance of the dopant is about 500–2500 nm even with the alloying element content C exceeding $C_c \approx 16$ vol%, so the most of these particles do not contact each other;

4) quantum-mechanical tunneling is significant at the distances of about the electron wavelength (≈ 6 nm) and can not noticeably contribute to conductivity at the distances more than 100 nm;

5) the experiment of laser fitting [15] has shown that the first endless conducting cluster is not formed even when $C > C_c$;

6) the infrared and optical spectra of the powders of the glass and the dopant have substantial difference before and after baking [41];

7) the resistance of the shortest (from contact to contact) chain of the RuO_2 particles contacting each other is much higher than the resistance of the thick-film resistor doped when $C \approx C_c \approx 16$ vol%;

8) the Ru atoms diffuse into the glass at the depth of more than $1\,\mu$m during baking (see Fig. 6, *a* in [42]) and resistivity of the glass varies by more than 12 orders due to this process (see Fig. 6 of [42]).

The DSG composition was analyzed by the energy-dispersive spectroscopy by Johnson et al. [29] to detect separate particles of lead ruthenate, CuBi ruthenate and zirconium silicate and specify their crystal structure by means of electron difraction. It was shown that the glass matrix contains Pb and Si (Fig. 7 in [29]). But, unfortunately, no distinctive feature like a size, a shape or contrast was detected so as to identify particles of different phases. The minimum particle size was 5 nm in the samples sintered at 825 °C (the baking time of 8 min), while in the sample sintered at 875 °C (for 12 min) the minimum particle size was ~ 20 nm. It indicates coarsening of the particles during baking. It can be presumed that dark areas of the Figures 7–9 in [29] are particles of an dopant. The similar conclusion was made by Hrovat et al. (the Figures 1, 2, 4 and 6 in [27]). It is clearly seen on these figures that the ligature particles do not contact each other and do not form a continuous conducting chain (an endless conducting cluster). This results well complies with the conclusions by Adachi et al [44].

No contact between the ligature particles is also confirmed in our samples by analysis of the distribution of the elements on the surface of the DCG of the composition 2 by energy-dispersive spectroscopy (Fig. 6). Fig. 7 shows the full spectrum of energy-dispersive analysis of the DCG of the composition 2.

In order to understand a mechanism of electrical conductivity of the thick-film resistors, Abe et al. [43,45] have studied mutual diffusion of atoms from the RuO_2 layer into the glass, and vice versa. It was reported that the rhutenium atoms diffused into the glass for the depth of more than $1\,\mu$m, whereas the glass thickness between the particles in the DSG was $1 - 2\,\mu$m, thereby meaning quite even doping of the entire glass layer. However, the authors have not studied a relation between such glass doping and electrical conductivity of the resistors. At the same time, the diffusion length in [43,45] substantially differs from the diffusion length determined in [37–39]. This diversion may be related to a different compositions of the studied glasses.

Therefore, a new approach to analysis of electrical conductivity in the DSG [36,40,46] was proposed using the glasses of the known (and simplest) composition. This approach is based on the following assumptions:

1) the Ru atoms from RuO_2 (or of other dopants) diffuse into the silicate glass and form an impurity area near the top of the valence band of the glass;

2) with increase of the temperature the impurity area is shifted towards the valence band of the glass due to an electron-phonon bond [47];

3) the silicate glass has nanocrystals that originate spontaneously and act as centers of localization of the charge carriers (holes);

4) these nanocrystals experience structural phase transitions at the high temperatures, which finally shifts the impurity area into a band gap of the glass, thereby changing the resistivity and the Seebeck coefficient of the DCG;

5) the DSG conductivity is a result of joint action of a jump (on the nanocrystals) and an activation (on the impurity area) mechanism.

The result shown on the figures 6 and 7 confirm these assumption by showing that it is the composition and the microstructure of the glass varying during doping and the

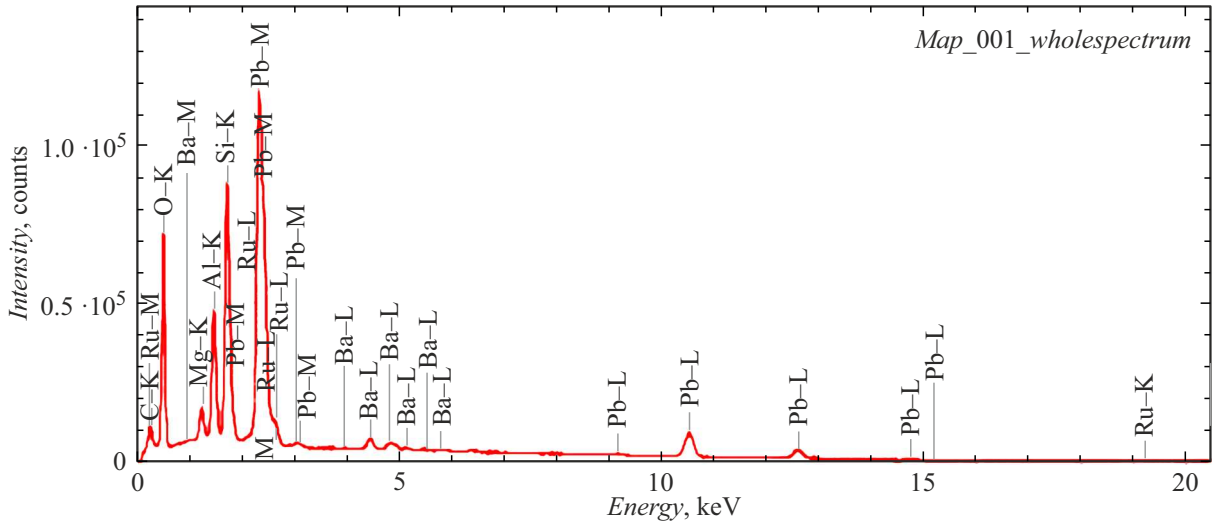

Figure 7. Content of the components in the glass of the composition 2 as per the EDS analysis.

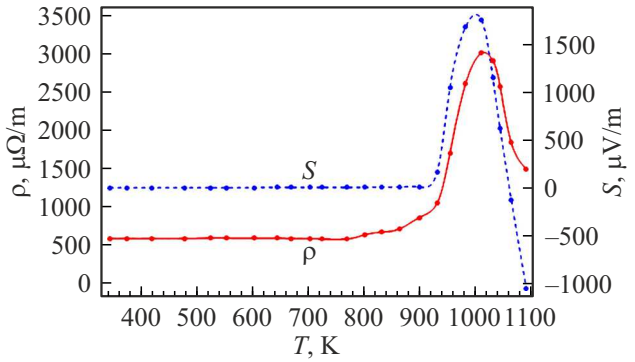

Figure 8. Resistance depending on the temperature for the doped glass 2 [46].

change of the microstructure (the distance between the atoms) during strain that have a decisive affect on the value of the thermoEMF and the resistance of the DSG. Fig. 6 shows that the RuO_2 particles are arranged from each other at the distances of about several μm even with the ligature content of 30 mass% (which corresponds to the volume content of about 16 %) and there is no direct contact between them. At the same time, as follows from the X-ray diffraction pattern, the nanocrystals with the sizes of 1−2 nm occupy about 50 % of the glass volume and the average distance between them is also about 1−2 nm. Therefore, the jumps (in essence, tunneling) with a variable length of the charge carriers between these nanocrystal significantly contribute to the conductivity. But only the jump mechanism is not enough to explain, for example, the DSG hole conductivity, when the ligature $Bi_2Ru_2O_7$ has electron conductivity, as well as a minimum of the resistance near the room temperature (Fig. 8). Therefore, explaining the observed temperature dependence of the resistance and the coefficient of the thermoEMF of the DSG required the jumps with the variable length and activation conductivity on the impurity area [46]. No direct contact between the RuO_2 particles means that the changes of the thermoEMF and the resistance are not related to changes of the area of the contacting surfaces of the ligature particles but are caused by local changes of the length and orientation of the atom bonds in the glass itself (i.e., finally, of a degree of overlapping of the wave functions of the charge carriers) during strain.

Fig. 7 shows an elementary composition of the DSG 2, which is obtained by the energy-dispersive spectroscopy. It is clear that the final elementary composition of the DSG is close to the initial composition of this compound (Table 2). Let us note that neither of the glasses, whose compositions are given in Table 2 has up to now been studied for tensometric applications and optimized from this point of view. Therefore, it can be expected that studying the glasses of the other compositions will detect materials with the strain gauge coefficient that is noticeably higher than those of Table 2.

Unfortunately, the nature of high strain sensitivity of the DSG and influence of the glass composition thereon are still unknown. At the same time, the situation is complicated by the fact [48] that it is unknown whether the thermoEMF is generated at a contact of two heterogeneous conductors [19,20] or within a volume of the uniform conductor [49,50]. The existing theory of thermoelectricity can describe a temperature dependence of the Seebeck coefficient only within the high temperatures, where it varies slowly and monotonically within changing the sign. There are also internal contradictions of the theory with the experiment as a quantitative difference of up to three orders of the magnitude and a qualitative difference as a sign change [48]. Despite this situation, the data of Fig. 5 show strong influence of the composition (and the structure, respectively) of the glass on the value of the

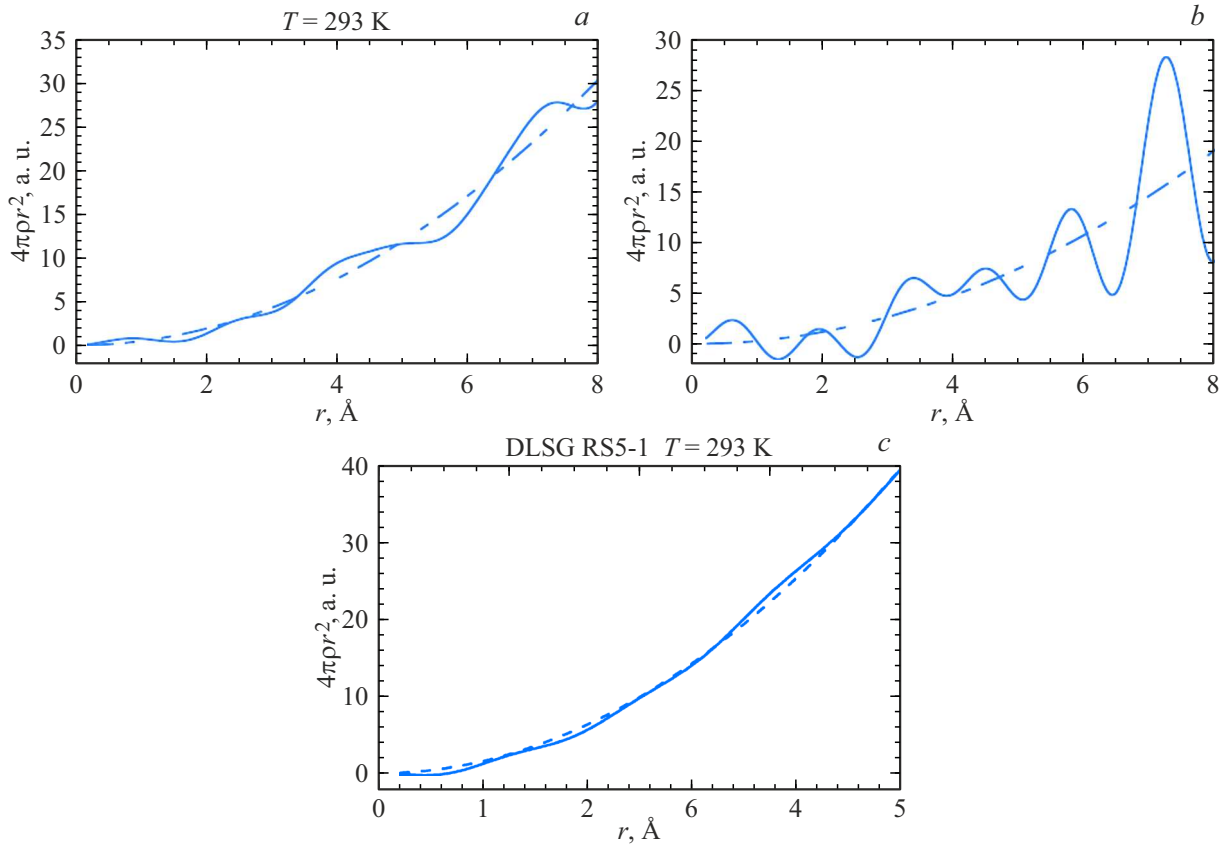

Figure 9. Functions of the radial distribution of the doped glasses of the compositions 1 (a), 2 (b) and 3(c).

thermoEMF U_T and the strain gauge coefficient GF_{UT} — the more complicated the composition, the lower U_T, but the higher GF_{UT}. This conclusion is confirmed by the functions of the radial distribution of the atoms (Fig. 9) in the studied DSGs, which are calculated from X-ray diffraction data [27,37]. Comparing these graphs of the functions of radial distribution in the DSGs with the data of Table 2 shows that the least order in the atom arrangement (the dashed parabola means close to the gases) observed in the DSG 3 results in the least value of the resistance R, the strain gauge coefficient of the resistance GF_R, the thermoEMF U_T and the least Seebeck coefficient S. At the same time, the strain gauge coefficient GF_{UT} is high and the ratio GF_{UT}/GF_R is also high (Table 2).

In the glass 2 that has the highest order in the atom arrangement, the situation is intermediate. Thus, it can be concluded that the composition of the glasses and their atom arrangement provide different results, which are often contrary to each other. Influence of the doped glasses on the studied parameters and these problems shall be studied in more detail from a physical point of view, while in practice it is important that the condition $GF_{UT} \gg GF_R$ is met. One of the possible explanations of the high sensitivity of the thermoEMF to strain in comparison to the resistance can be a difference of the density of the electron states (the Mott formula for the metals) [51]:

$$\sigma = \int c(E)\left(-\frac{df(E)}{dE}\right)dE,$$

$$\sigma S = -\frac{k_B}{e}\int \frac{E-\mu}{k_B T}\, c(E)\left(-\frac{df(E)}{dE}\right)dE, \qquad (5)$$

where k_B — the Boltzmann constant, e — the electron charge, $c(\mu) = e^2 D(E)N(E)$, $D(E)$ — the diffusion constant of the charge carriers (holes or electrons) and $N(E)$ — the density of electron states. For the metals, these formulas can be simplified to

$$\sigma_S = -\frac{\pi^2 k_B^2 T}{3e}\frac{c'(\mu)}{c(\mu)}, \quad \sigma = c(\mu). \qquad (6)$$

It is clear from the equation (6) that in case of sharp variation of $N(E)$ the logarithmic derivative $N'(E)/N(E)$ and S, respectively, vary with strain stronger than σ that linearly depends on $N(E)$. In accordance with our previous studies [52,53], the similar situation occurs in the doped silicate glass (Fig. 10). We have reported narrowing of the band gap ($10 - 50$ meV) when doping with impurities, which is separated from the valence band of the glass by a small pseudogap of $10 - 30$ meV. The density of states around the impurity area is very high [about 10^{22} eV^{-1}cm^{-3}], which

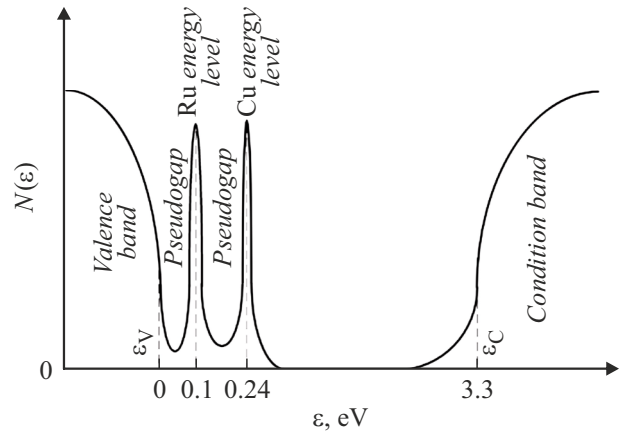

Figure 10. Density of states in the silicate glass jointly doped by RuO_2 and CuO [53].

results in a sharp change of the density of states in the pseudogap. $N'(E)/N(E) \approx (30-100)\,\mathrm{eV}^{-1}$.

Influence of strain on thermoelectric properties of Mg_2Si was studied by a density functional theory [54]. It was found that the Seebeck coefficient and the energy factor significantly varied with application of strain (compression or tension) due to modulation of the width of the band gap. The material is still a semiconductor with strain up to 3%. The recent theoretical study of Zosiamliana et al. has reported influence of compressive pressure on the density of electron states and the width of the band gap in Na_2SiO_3 [55]. It is shown that the width of the band gap does not change monotonically — it increases with increase of the pressure to 20 GPa, then decreases with the pressure below 40 GPa and increases again. The changes in the width of the band gap are directly related to the change of the density of electron states, which in turn changes the Seebeck effect (the thermoelectric energy factor). The results from [54] demonstrate a wide spectrum of effects of strain on the density of electron states, the width of the band gap and the Seebeck coefficient of the various materials.

Conclusion

The thick-film thermoelectric structures have high (in 20–120 times higher than the resistance of the same samples) sensitivity to strain. The composition and the structure of the sensitive layer (of the doped glass) of the thermocouple substantially affect the final characteristics of the strain sensor: the higher disorder in the material structure, the less the numerical value of the thermoEMF, but the higher its sensitivity to strain. The high sensitivity of the thermoEMF to strain as compared to the resistance occurs due to the narrow impurity area that is created during doping and arranged near the valence band of the glass. The thermoelectric strain sensors based on oxides ensure technological flexibility and have high reliability that is confirmed by mass production and use of the thick-film resistor for more than 50 years in various electronic equipment (including special equipment).

Funding

The study is performed in the framework of a joint Belarus-Uzbek project that is financially supported by Ministry of Higher Education, Science and Innovation of Uzbekistan (the grant № IL-482109667) and Belarus Republican Foundation for Fundamental Research (the grant № F22UZB-056).

Conflict of interest

The authors declare that they have no conflict of interest.

References

[1] J. Friden. *Handbook of Modern Sensors. Physics, Design and Applications*. 4th ed. (Springer, 2010)
[2] A.S. Fiorillo, C.D. Critello, A.S. Pullano. Sensors Actuators A: Phys., **281**, 156 (2018). DOI: 10.1016/j.sna.2018.07.006
[3] M.J. McGrath, C. Ni Scanaill. *Sensor Technologies. Healthcare, Wellness and Environmental Applications* (Apress Open, 2014)
[4] J.X.J. Zhang, K. Hoshino. *Molecular Sensors and Nanodevices* (Elsevier, 2019), DOI: 10.1016/C2017-0-02290-5
[5] Y. Zhao, Y. Liu, Y. Li, Q. Hao. Sensors, **20**, 5826 (2020). DOI: 10.3390/s20205826
[6] H. Trietley. *Strain Gauges: Basic Operating Principles, Materials, and Properties.* https://control.com/technical-articles/strain-gauges-basic-operating-principles-materials-and-properties/
[7] K. Arshak, D. Morris, A. Arshak, O. Korostynska. J. Mater. Sci.: Mater Electron, **17**, 767 (2006). DOI: 10.1007/s10854-006-0013-4
[8] J. Shu, R. Yang, Y. Chang, X. Guo, X. Yang. J. Alloys Compounds, **879**, 160466 (2021). DOI: 10.1016/j.jallcom.2021.160466
[9] Y. Cui, X. Li, T. Zhang, W. Ding, J. Yin. Sensors, **22**, 7595 (2022). DOI: 10.3390/s22197595
[10] R. Ottermann, D. Klaas, F. Dencker, M.C. Wurz, D. Hoheisel, P. Rottengatter, T. Kruspe. *Direct Deposition of Thin-Film Strain Gauges with a New Coating System for Elevated Temperatures*. In Proceed. 2020 IEEE SENSORS, Rotterdam, The Netherlands, 25–28 October 2020, p. 1–4
[11] Y. Zhao, Y. Li, Y. Wu, G. Ding, C. Zhang. IEEE Sensors J., **24** (7), 2024, 01 (2024). DOI: 10.1109/JSEN.2024.3363510
[12] M. Prudentiziati (Ed.), *Handbook of Sensors and Actuators: Thick-films Sensors* (Elsevier, 1994), v. 1.
[13] Y. Zheng, J. Atkinson, R. Sion. J. Phys. D: Appl. Phys., **36**, 1153 (2003). DOI: 10.1088/0022-3727/36/9/314
[14] M. Hrovat, J. Holc, D. Belavič, S. Šoba. J. Mater. Sci. Lett., **13**, 992 (1994). DOI: 10.1007/BF00701448
[15] G. Abdurakhmanov. World J. Cond. Matter Phys., **4** (3), 166 (2014). DOI: 10.4236/wjcmp.2014.43021

[16] G. Abdurakhmanov. *Electrical conduction in doped silicate glass (thick film resistors)*. In: *New Insights into Physical Sciences* (London-Hooghly, Book Publishers International, 2020), v. 4, p. 47–71. DOI: 10.9734/bpi/nips/v4
[17] S.P. Bogdanov, V.V. Kozlov, A.P. Shevchik, A.S. Dolgin. Refractories and Industrial Ceramics, **60** (4), 405 (2019). DOI: 10.1007/s11148-019-00376-0
[18] Electronic media. Available at: http://www.glasswork.ru/auxpage_glass_properties?ysclid=lzp77nl4jb353096302.
[19] A.G. Samoilovich, L.L. Korenblit. UFN, **49** (2), 243 (1953) (in Russian).
[20] K.A. Putilov. *Kurs fiziki*. V trekh tomakh. V. 2 (Gosudarstvennoe izd-vo fiziko-matematicheskoi lit-ry, M., 1963) (in Russian).
[21] M. Hrovat, D. Belavič, Z. Samaržija, J. Holc. J. Mater. Sci., **36**, 2679 (2001). DOI: 10.1023/a:1017908728642
[22] M. Hrovat, D. Belavič, Z. Samaržija, J. Holc. *An Investigation of Thick-Film Resistor, Fired at Different Temperatures, for Strain Sensors*. 24th Int. Spring Seminar on Electronics Technology. May 5–9, 2001, Calimanesti-Caciulata, Romania. Conference Proceedings, 32–36
[23] M. Hrovat, J. Holc, D. Belavič, S. Šoba. J. Mater. Sci. Lett., **14**, 584 (1995).
[24] M. Hrovat, D. Belavič, H. Uršič, J. Kita, J. Holc, S. Drnovšek, J. Cilensek, M. Kosec, R. Moos. *An Investigation of Thick-film Materials for Temperature and Pressure Sensors on Self-constrained LTCC Substrates*. IEEE 2008 2nd Electronics Systemintegration Technology Conference – Greenwich, Sept. 01–04, 2008. Proc. p. 339–346. DOI: 10.1109/estc.2008.4684372
[25] Y. Ma, J. Chen, M. Li. *$Bi_2Ru_2O_7$ Conductive Phase and its Effects on the Gauge Factor of Ru-based Thick-film Resistors*. Proceedings of the 2006 IEEE Intern. Conf. on Information Acquisition. August 20–23, 2006, Weihai, Shandong, China. p. 245–248.
[26] C. Song, D.V. Kerns, Jr., J.L. Davidson, W. Kang, S. Kerns. *Evaluation and Design Optimization of Piezoresistive Gauge Factor of Thick-film Resistors*. IEEE Proceedings of the SOUTHEASTCON '91, p. 1106. DOI: 10.1109/secon.1991.147935
[27] M. Hrovat, G. Drat'ic, J. Holc, D. Belavič. J. Materials Sci. Lett., **14**, 1048 (1995).
[28] M. Prudenziati. *Piezoresistive effects in thick film resistors: 30 years after*. STAMPA, (2005), p. 207–216. (Intervento presentato al convegno Sensors and Microsystems tenutosi a Ferrara nel 8–11 February 2004)
[29] F. Johnson, G.M. Crosbie, W.T. Donlon. J. Mater. Sci.: Mat. In Electron., **8** (1), 29 (1997).
[30] M. Prudenziati, B. Morten, F. Cilloni, G. Ruffi. Sensors and Actuators, **19**, 401 (1989).
[31] M. Hrovat, J. Holc, Z. Samardžija. J. Mater. Sci. Lett., **20**, 701 (2001).
[32] C. Grimaldi1, P. Ryser, S. Strässler. *Anisotropic random resistor networks: a model for piezoresistive response of thick-film resistors* (arxiv:cond-mat/0203612v1 [cond-mat.dis-nn] 29 Mar. 2002)
[33] S. Vionnet Menot. *Low firing temperature thick-film piezoresistive composites — properties and conduction mechanism* (PhD Thesis, Lausanna, 2005)
[34] O. Correa, P.P. de Abreu Filho, S. Moshkalev, J. Swart. Sensors, **22**, 3256 (2022). DOI: 10.3390/s22093256
[35] C. Ferrero. *Proposed theoretical models for thick film transport mechanisms: example of thick film strain gauges on enamelled steels* (2022), 51 p. https://www.researchgate.net/publication/358042608
[36] J.M. Ziman. *Models of Disorder* (Cambridge University Press, Cambridge, 1979)
[37] M. Totokawa, T. Tani, H. Azuma, A. Takeichi, R. Asahi. J. Am. Ceram. Soc., **93** (10), 3312 (2010). DOI: 10.1111/j.1551-2916.2010.03844.x
[38] M. Totokawa, T. Tani, M. Yoshimura, S. Yamashita, K. Morikawa, Y. Mitsuoka, T. Nonaka. J. Am. Ceram. Soc., **93** (2), 481 (2010). DOI: 10.1111/j.1551-2916.2009.03403.x
[39] M. Totokawa, T. Tani, S. Yamashita, K. Morikawa, Y. Mitsuoka, H. Makino. Int. J. Appl. Ceram. Technol., **6** (2), 195 (2009). DOI: 10.1111/j.1744-7402.2008.02325.x
[40] G. Abdurakhmanov. WJCMP, **1** (2), 19 (2011). DOI: 10.4236/wjcmp.2011.12004
[41] G. Abdurakhmanov. WJCMP, **1** (1), 1 (2011). DOI: 10.4236/wjcmp.2011.11001
[42] T. Yamaguchi, Y. Nakamura. J. Am. Ceram. Soc., **78** (5), 1372 (1995).
[43] O. Abe, Y. Taketa. J. Phys. D: Appl. Phys., **24**, 1163 (1991).
[44] K. Adachi, H. Kuno. J. American Ceramic Soc., **80** (5), 1055 (1997). DOI: 10.1111/j.1151-2916.1997.tb02946.x
[45] O. Abe, Y. Taketa, M. Haradome. Electrical Eng. Jpn., **110** (1), 21 (1990).
[46] G. Abdurakhmanov. *Electrical conduction in doped silicate glass* (thick film resistors. In New Insights into Physical Sciences (London-Hooghly, Book Publishers International, 2020), v. 4, p. 47–71. DOI: 10.9734/bpi/nips/v4
[47] K.P. O'Donnell, X. Chen. Appl. Phys. Lett., **58** (25), 2924 (1991).
[48] G. Abdurakhmanov, G.S. Voxidova, D. Rai. *Modern Physics of Thermoelectric Phenomena — Achievements and Problems*. In New Materials and Devices for Thermoelectric Power Generation (IntechOpen, 2023)
[49] K. Seeger. *Semiconductor Physics* (Springer, Berlin, 2004)
[50] D.K.C. MacDonald. *Thermoelectricity: An Introduction to the Principles* (Dover Publications, Minneola, NY., 2016)
[51] M. Cutler, N.F. Mott. Phys. Rev., **181** (3), 1336 (1969). DOI: 10.1103/PhysRev.181.1336
[52] G. Abdurakhmanov, V.I. Shimanski, B. Onsengendler, B. Umirzahov, A.N. Urokov. Tech. Phys., **66** (2), 269 (2021). DOI: 10.1134/S106378422102002X
[53] G. Abdurakhmanov, A. Dekhkonov, M. Tursunov, D. Tashmukhamedova. Phys. Sci. Intern. J., **27** (6), 5 (2023). DOI: 10.9734/PSIJ/2023/v27i6806
[54] K. Kaur, R. Kumar. Chin. Phys. B, **26** (6), 066401 (2017). DOI: 10.1088/1674-1056/26/6/066401
[55] R. Zosiamliana, Lalrinkima, B. Chettri, G. Abdurakhmanov, M.P. Ghimire, D.P. Rai. RSC Adv., **12**, 12453 (2022). DOI: 10.1039/D2RA01125E

Translated by M.Shevelev